Available online at www.sciencedirect.com

SciVerse ScienceDirect

Acta Materialia 59 (2011) 7634–7644

Acta MATERIALIA

www.elsevier.com/locate/actamat

Diffusion kinetics in aluminium–gold bond contacts from first-principles density functional calculations

Christian M. Ulrich [a,*], Adham Hashibon [a], Jiří Svoboda [b], Christian Elsässer [a], Dirk Helm [a], Hermann Riedel [a]

[a] *Fraunhofer Institut for Mechanics of Materials IWM, Wöhlerstr. 11, 79108 Freiburg, Germany*

[b] *Institute of Physics of Materials, Academy of Sciences of the Czech Republic, Zizkova 22, CZ-616 62 Brno, Czech Republic*

Received 10 March 2011; received in revised form 10 August 2011; accepted 14 August 2011
Available online 15 October 2011

Abstract

A common joining method in microelectronics is thermosonic bonding of gold wires to aluminium pads deposited on the integrated circuit. In the interface between the wire and the pad a number of intermetallic compounds Al_xAu_y can develop, which significantly affect the mechanical properties and corrosion resistance of the bonds. Based on Onsager's extremal principle of irreversible thermodynamics, the present paper describes the evolution of the intermetallic phases. This macroscopic model contains several thermodynamic and kinetic parameters, some of which are not available from databases. As an alternative to often cumbersome experiments, density functional theory is applied to calculate the formation energies of the phases and of atomic vacancies, as well as the vacancy migration energies in $AlAu_4$. To derive tracer diffusion coefficients from the atomistic vacancy jump rates, one must take peculiarities of the $AlAu_4$ lattice into account: the vacancy migration energy between certain gold sites is found to be rather low, but these low-energy jumps are arranged in closed triangles and, therefore, do not provide paths for long-range diffusion of gold atoms. However, together with two other types of jumps with still moderate migration energies, a contiguous network of diffusion paths for gold becomes possible. Since the diffusion of aluminium in $AlAu_4$ requires the generation of high- energy anti-site defects (at least temporarily), aluminium is expected to move very slowly, but no final solution is provided.

Keywords: Bonding; Diffusion; Intermetallic compounds; Al–Au; Growth kinetics

1. Introduction

Contacts of gold wires on aluminium bond pads are of special interest in microelectronics due to their widespread use in fine-pitch applications [1]. During the bonding process and subsequent manufacturing steps, solid-state phase reactions lead to the formation and growth of intermetallic Al–Au compounds in the wire-bond interface [2]. This may continue during the normal usage of the device, especially at elevated temperatures, and it may be associated with the formation of voids, microcracks, interface decohesion and the eventual failure of the wire bond [3–6]. The kinetics of the solid-state phase reactions are controlled to a large extent by diffusion processes in the bulk volume and along the grain and phase boundaries. Hence an investigation of the atomistic diffusion processes is vital for a better understanding of the degradation mechanism of wire bonds and this understanding will help to improve the reliability of the devices. Electric currents may also enhance microstructural changes due to electromigration [7], an aspect which is not covered by the present paper.

In close-packed metals, vacancy-mediated diffusion mechanisms are dominant, although along grain or phase boundaries other mechanisms, like interstitial mediated processes, may also be important [8]. In general, the diffusion coefficients of the participating species are different, which

* Corresponding author. Tel.: +49 (0) 761 5142 260.
E-mail address: christian.markus.ulrich@iwm.fraunhofer.de (C.M. Ulrich).

1359-6454
doi:10.1016/j.actamat.2011.08.021

causes unbalanced matter transport and net fluxes of vacancies across the phases at the interface. This is known as the Kirkendall effect [9] and has observable consequences, such as relative movements of the atomic lattice (Kirkendall shift) or supersaturation of vacancies, leading to the formation of pores at the transition between two phases [10,11].

The Au–Al system exhibits a rich phase diagram with a number of stable low-temperature intermetallic phases [12]. Those which are most relevant to wire bonding are listed in Table 1, along with their crystallographic data. Note that the α- and β-$AlAu_2$ phases are seldom distinguished in the literature. Some experimental studies on Al–Au phase kinetics have found all of these intermetallics to form [4,13–16], while others have only reported subsets [17–20]. This may suggest a strong dependence on manufacturing conditions and alloy composition.

There have been different approaches for simulations of the reaction kinetics of layered systems of stoichiometric phases, notably using Dictra [21] or similar approaches to solve classical phenomenological equations, or applying a thermodynamic extremal principle [22] to derive the phase evolution on a macroscopic scale [23]. In both cases, one has to rely on thermodynamic and kinetic data, such as phase formation energies and diffusion coefficients, which need to be supplied by experimentation or other means.

The diffusivities of both Al and Au in the intermetallic phases, which strongly control phase kinetics and intermetallic growth, are unknown, partly because of the lack of a suitable aluminium tracer isotope. Diffusion couple experiments with inert marker particles to obtain the Kirkendall velocity and marker experiments with ^{198}Au have been done for gold-rich solid solutions [29], but, to the best of our knowledge, mobilities and diffusion mechanisms in the intermetallic compounds have not so far been reported.

In the present work, the evolution of the intermetallic phases is described by a combination of models on three different length scales. On the smallest scale (Section 2.1), quantum–mechanical density functional theory (DFT) is used to calculate the formation energies of the intermetallic phases and of vacancies. The vacancy migration energies and the vibration frequencies of the atoms around a vacancy are also calculated using DFT. These quantities are needed in the atomistic diffusion theory – i.e. on the intermediate length scale – to calculate tracer diffusion coefficients (Sections 2.2 and 3.4), which in turn are used on the macroscopic level, where a thermodynamic–kinetic model for the evolution of the phases is established based on Onsager's principle of maximum dissipation rate [23,30,31] (Section 2.3).

There are few studies of DFT for the Al–Au system [32], and those do not consider phase formation energies or defect and diffusion properties. In the present study, our focus lies on the phase $AlAu_4$, as failures in bond contacts by delamination or severely diminished strength after ageing often occur in the boundary between the $AlAu_4$ and Al_3Au_8 phases or between $AlAu_4$ and the gold ball [11].

Table 1
Crystallographic data of low-temperature Al–Au intermetallics. In addition to the space group and lattice parameters, the Wyckoff positions and reduced coordinates of basis atoms are shown. The latter are from the DFT calculations done in this work.

Compound	Lattice parameters	Position	Relaxed coordinates
Al_2Au	$a = b = c = 4.2407$Å,	Al 2**c**	(0.25, 0.25, 0.25)
Fm-3 m (225)	$\alpha = \beta = \gamma = 60°$,	Au 1**a**	(0.0, 0.0, 0.0)
	from [24]		
AlAu	$a = 6.415$Å,	Al 2**e**	(0.1820, 0.25, 0.5798)
$P2_1/m$ (11)	$b = 3.331$Å,	Al 2**e**	(0.6803, 0.25, 0.9532)
	$c = 6.339$Å,	Au 2**e**	(0.0240, 0.25, 0.1919)
	$\beta = 93.04°$,	Au 2**e**	(0.4946, 0.25, 0.3121)
	$\alpha = \gamma = 90°$,		
	from [25]		
α-$AlAu_2$	$a = 6.715$Å,	Al 4**c**	(0.1315, 0.25, 0.2253)
Pnma (62)	$b = 3.219$Å,	Au 4**c**	(0.6478, 0.25, 0.5773)
	$c = 8.815$Å,	Au 4**c**	(0.0900, 0.25, 0.6126)
	$\alpha = \beta = \gamma = 90°$,		
	from [26]		
β-$AlAu_2$	$a = 8.801$Å,	Al 2**a**	(0.0, 0.0, 0.0)
Pnnm (58)	$b = 16.772$Å,	Al 4**g**	(0.9806, 0.2014, 0.0)
	$c = 3.219$Å,	Al 4**g**	(0.0277, 0.4011, 0.0)
	$\alpha = \beta = \gamma = 90°$	Au 4**g**	(0.3442, 0.0136, 0.0)
	from [26]	Au 4**g**	(0.3596, 0.1874, 0.0)
		Au 4**g**	(0.3269, 0.4046, 0.0)
		Au 4**g**	(0.3626, 0.6061, 0.0)
		Au 4**g**	(0.3306, 0.7879, 0.0)
Al_3Au_8	$a = b = c = 14.72$Å,	Al 2**b**	(0.0, 0.0, 0.0)
R-3c (167)	$\alpha = \beta = \gamma = 30.42°$	Al 4**c**	(0.1557, 0.1557, 0.1557)
	from [27]	Al 6**e**	(0.9339, 0.5661, 0.25)
		Au 4**c**	(0.2173, 0.2173, 0.2173)
		Au 4**c**	(0.0638, 0.0638, 0.0638)
		Au 12**f**	(0.0035, 0.6490, 0.2962)
		Au 12**f**	(0.1205, 0.6516, 0.3840)
$AlAu_4$	$a = b = c = 6.9227$Å,	Al 4**a**	(0.6875, 0.6875,0.6875)
$P2_13$ (198)	$\alpha = \beta = \gamma = 90°$	Au 4**a**	(0.0671, 0.0671, 0.0671)
	from [28]	Au 12**b**	(0.1342, 0.1999,0.4632)

2. Modelling methods

2.1. DFT calculation of configuration energies and migration barriers

Total energies of the intermetallic phases and of vacancies in these lattices are calculated by DFT [33,34], with the local density approximation for exchange correlation (LDA) [35]. The interaction of valence electrons with ionic cores is described with norm-conserving pseudopotentials [36]. Wave functions of the valence electrons are expanded on a mixed basis [37–39] of plane waves and additional localized functions for the *d*-states of Au. Boundary conditions are periodic along all three lattice directions. Brillouin-zone integrations in reciprocal space are carried out on *k*-point grids [40] with Gaussian broadening [41] of 0.2 eV (as given in Tables 2 and 3 for relaxations with and without vacancies, respectively). In Section 3.3 minimum energy paths and saddle point energies (see Fig. 1) are determined by means of the nudged elastic band (NEB) method [42].

Formation enthalpies ΔH_F of the intermetallic compounds Al_aAu_b were calculated according to

$$\Delta H_F[Al_aAu_b] = \frac{1}{a+b}\left(E[Al_aAu_b] - a\mu_{Al}^{fcc} - b\mu_{Au}^{fcc}\right) \quad (1)$$

where a and b are the number of aluminium and gold atoms in the cell, $E[Al_aAu_b]$ is the calculated energy of the cell, and $\mu_{Al}^{fcc} = E[fcc - Al]$ and $\mu_{Au}^{fcc} = E[fcc - Au]$ are the chemical potentials of aluminium and gold in their bulk face-centred cubic (fcc) phases, as calculated with the same DFT method.

The formation energy for a vacancy is calculated as the energy that is needed to remove one atom from the ideal bulk structure, placing it into a reference structure where the chemical potentials for gold and aluminium are known as μ_{Au} and μ_{Al}, respectively. It follows that the vacancy formation energies in an intermetallic compound Al_aAu_b can be calculated as [43,44]:

$$\begin{aligned} E_V^{Al}[Al_aAu_b] &= E[Al_{a-1}Au_b] + \mu_{Al} - E[Al_aAu_b] \\ E_V^{Au}[Al_aAu_b] &= E[Al_aAu_{b-1}] + \mu_{Au} - E[Al_aAu_b] \end{aligned} \quad (2)$$

Here, $E[Al_aAu_b]$ is the energy of the relaxed bulk cell, and $E[Al_{a-1}Au_b]$ and $E[Al_a\ Au_{b-1}]$ are the energies of a cell from which an aluminium or gold atom, respectively, has been removed. μ_{Al} and μ_{Au} can vary according to the chemical conditions, and are given by

$$\begin{aligned} \mu_{Al} &= \mu_{Al}^{fcc} + \Delta\mu_{Al} \\ \mu_{Au} &= \mu_{Au}^{fcc} + \Delta\mu_{Au} \end{aligned} \quad (3)$$

$\Delta\mu_{Al}$ gives the deviation of the chemical potential of aluminium in the intermetallic from its value in equilibrium with the fcc-Al phase, and $\Delta\mu_{Au}^{fcc}$ likewise for the chemical potential of gold and the fcc-Au phase. With the relation

$$a\Delta\mu_{Al} + b\Delta\mu_{Au} \equiv (a+b)\Delta H_F[Al_aAu_b] \quad (4)$$

only one independent variable remains, and vacancy formation energies can be calculated over a range of chemical conditions. For the intermetallic compound i, this range is bounded on the aluminium-rich side by the thermodynamic equilibrium with compound $i-1$ and on the gold-rich side by the equilibrium with compound $i+1$ (e.g. if i denotes the compound $Al_3\ Au_8$,$i-1$ would be $AlAu_2$ and $i+1$ would be $AlAu_4$; see Fig. 3). The corresponding $\Delta\mu_{Al}$ and $\Delta\mu_{Au}$ in the extreme cases can be calculated by application of the double tangent rule and are given by

$$\begin{aligned} \Delta\mu_{Au} &= \Delta H_{F,i} + \frac{\Delta H_{F,i+1} - \Delta H_{F,i}}{x_{i+1} - x_i}(1 - x_i) \\ \Delta\mu_{Al} &= \Delta H_{F,i} - \frac{\Delta H_{F,i+1} - \Delta H_{F,i}}{x_{i+1} - x_i}x_i \end{aligned} \quad (5)$$

for gold-rich conditions and

$$\begin{aligned} \Delta\mu_{Au} &= \Delta H_{F,i} + \frac{\Delta H_{F,i} - \Delta H_{F,i-1}}{x_i - x_{i-1}}(1 - x_i) \\ \Delta\mu_{Al} &= \Delta H_{F,i} - \frac{\Delta H_{F,i} - \Delta H_{F,i-1}}{x_i - x_{i-1}}x_i \end{aligned} \quad (6)$$

for aluminium-rich conditions, with x_i denoting the molar fraction of gold in compound i.

During relaxation of the defect structures, the size of the cell is kept fixed.

Besides the vacancy formation energies, the migration energies and the atomic vibration frequencies are also needed for the calculation of the diffusion coefficients. The migration energies are calculated using the NEB method [42] to find the path with the lowest saddle point

Table 2
Formation enthalpies of the low-temperature Al–Au-phases, as calculated with Eq. (1), for the two plane wave cut-off energies E_{cut}. The k-point sampling used in each case is also shown. The results indicate that the formation energies converge well for $E_{cut} = 218$ eV.

		ΔH_F(kJ/mol)	
Compound	k_{xyz}	$E_{cut} = 218$ eV	$E_{cut} = 300$ eV
Al_2Au	$32 \times 32 \times 32$	−46.9	−46.6
AlAu	$12 \times 12 \times 12$	−43.4	−43.2
α-$AlAu_2$	$8 \times 8 \times 8$	−36.3	−36.3
β-$AlAu_2$	$4 \times 2 \times 8$	−35.7	−35.7
Al_3Au_8	$4 \times 4 \times 4$	−31.0	−31.0
$AlAu_4$	$8 \times 8 \times 8$	−23.3	−23.3

Table 3
Vacancy formation energies calculated for sc and fcc supercells; d_V: inter-vacancy distance. Letters in parentheses indicate the Wyckoff position of the sites as given in Table 1. Note that, for the AlAu system, there are two non-equivalent Wyckoff **e** sites for both Al and Au. These values were calculated from Eq. (2) with $\Delta\mu_{Al} = \Delta\mu_{Au} = 0$. To account for the influence of Au-rich or Al-rich conditions, appropriate values of $\Delta\mu$ from Eq. (5) or (6) must be added (see Fig. 4).

	Al_2Au		AlAu	$AlAu_4$	
	sc	fcc		sc	fcc
k_{xyz}	$6 \times 6 \times 6$	$4 \times 4 \times 4$	$8 \times 8 \times 8$	$8 \times 8 \times 8$	$4 \times 4 \times 4$
d_V (Å)	5.97	8.45	3.33	6.92	9.79
E_V^{Al} (eV)	1.98 (**c**)	1.89 (**c**)	1.90 (**e**)	2.14 (**a**)	2.15 (**a**)
			1.79 (**e**)		
E_V^{Au} (eV)	3.11 (**a**)	3.19 (**a**)	1.88 (**e**)	0.628 (**a**)	0.629 (**a**)
			1.89 (**e**)	0.580 (**b**)	0.551 (**b**)

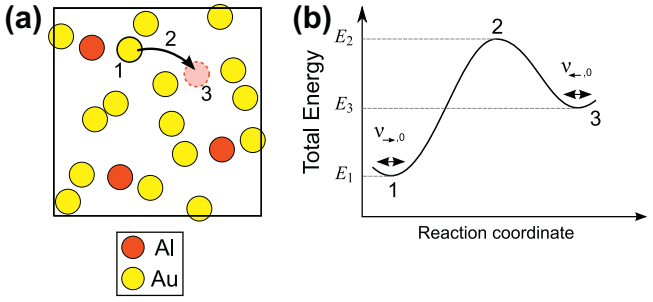

Fig. 1. (a) A schematic of an atomic jump process in a unit cell of the intermetallic compound $AlAu_4$, shown as a projection in the (010) direction. In this case, a jump of a gold atom to an adjacent aluminium vacancy is presented. (b) The corresponding energy path, indicating energy at the beginning (E_1) and end (E_3) of the jump and the saddle point energy E_2, is shown.

energy. The energy along such a path is shown schematically in Fig. 1. The values at the starting position, E_1, at the saddle point, E_2, and at the end position, E_3, are used later in the atomistic diffusion theory.

The so-called attempt frequency is calculated assuming a harmonic model as the frequency of the atom at the starting position:

$$\nu_{\rightarrow,0} = \frac{1}{2\pi}\sqrt{\frac{2\Delta E}{m\Delta x^2}} \tag{7}$$

with ΔE the difference in total energy between the initial state configuration and a configuration with the jumping atom displaced by Δx, and m the mass of the jumping atom ($m_{\mathrm{Au}} = 197$ u and $m_{\mathrm{Al}} = 27$ u). The attempt frequency for the backward jump, $\nu_{\leftarrow,0}$, is calculated analogously from the final state configuration and a configuration with displacement Δx of the jump.

2.2. Tracer diffusion coefficients from atomistic diffusion theory

The calculation of diffusion coefficients from the attempt frequencies and the activation energies of the elementary jump processes is a complicated task. In general, large-scale kinetic Monte Carlo simulations or equivalent methods are needed to solve the problem. Ordered intermetallic compounds pose special problems, which cannot be treated by the classical atomistic diffusion theory [45–48]. Since the approximate method to deal with these problems is especially designed for $AlAu_4$, it is better described in Section 3, where the results for the Al–Au intermetallic compounds are presented.

2.3. The phenomenological model for the reaction kinetics

For simulation of the reaction kinetics in a system of intermetallic phases like the weld joint between an aluminium bond pad and a gold wire, we use a phenomenological model due to Svoboda et al. [23]. The geometry of the model, shown in Fig. 2, is a simple one-dimensional arrangement of n planar layers of thickness $d_i (i = 1 \cdots n)$, in which diffusion by a vacancy mechanism occurs. Each of the layers consists of a perfect binary intermetallic bulk phase with fixed stoichiometric composition, as designated by the molar fraction of gold, $x_{\mathrm{Au},i}$. The terminal phases are taken to be the pure elements, their composition being $x_{\mathrm{Au},1} = 0$ on the aluminium side and $x_{\mathrm{Au},n} = 1$ on the gold side. The evolution of the system towards a state of thermodynamic equilibrium is governed by the diffusive fluxes of gold and aluminium atoms $j_{\mathrm{Al},i}$ and $j_{\mathrm{Au},i}$, respectively. Since the phases are assumed to be perfectly ordered stoichiometric compounds, the fluxes do not have gradients within the phases, and may vary discontinuously at phase boundaries. Such a situation can hardly be described by the standard diffusion equation, as proposed, for example, by Xu and Van der Ven [49]. As a consequence of the stoichiometry, there are no concentration gradients in the phases, and the thermodynamic factors

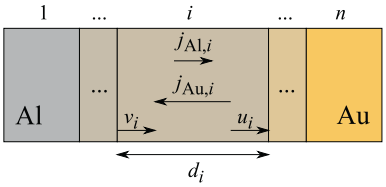

Fig. 2. Geometry of the phenomenological model [23] used in this work. The positive direction for the quantities flux (j) and velocity (u,v) is to the right.

assume infinite values. An alternative to using the diffusion equation was proposed in Refs. [22,23,50]. It is based on the principle of maximum entropy production, $Q = \max$, subject to the constraint $Q + \dot{G} = 0$, where G is the Gibbs energy of the system [30]. The Gibbs energy can be calculated from the molar Gibbs energies of the phases ${}^{m}G_i$. Its time derivative is

$$\dot{G} = \sum_{i=1}^{n} \frac{{}^{m}G_i \dot{d}_i}{\Omega_i} \tag{8}$$

For systems not too far from equilibrium, the total dissipation (or entropy production) rate Q is a positive definite quadratic form of the diffusive fluxes with the tracer diffusion coefficients as the material parameters [22,23,50]:

$$Q = \sum_{i=2}^{n-1} R_g T \Omega_i d_i \left[\frac{j_{\mathrm{Al},i}^2}{x_{\mathrm{Au},i} D_{\mathrm{Al},i}^*} + \frac{j_{\mathrm{Au},i}^2}{(1 - x_{\mathrm{Au},i}) D_{\mathrm{Au},i}^*} \right] \tag{9}$$

with T the absolute temperature, R_g the gas constant, Ω_i the molar volume of phase i, and $D_{\mathrm{Al},i}^*$ and $D_{\mathrm{Au},i}^*$ the tracer diffusion coefficients of aluminium and gold in phase i.

In cases in which the dissipation rate is quadratic in the fluxes, the principle of maximum entropy production leads to

$$-\frac{\partial}{\partial j_i}\dot{G} = \frac{1}{2}\frac{\partial}{\partial j_i} Q \tag{10}$$

with j_i denoting the fluxes $j_{\mathrm{Al},i}$ and $j_{\mathrm{Au},i}, i = 2 \ldots n-1$.

In order to carry out the differentiation of $\dot{G}$ in Eq. (8) with respect to the fluxes, one needs a relation between the thickening rate of the phases, $\dot{d}_i$, and the fluxes. From mass conservation arguments, one calculates the displacement rates of the left and right interfaces of phase i

$$\begin{aligned} u_i &= \frac{\Omega_i}{x_{\mathrm{Au},i} - x_{\mathrm{Au},i+1}} [(j_{\mathrm{Au},i} - j_{\mathrm{Au},i+1})(1 - x_{\mathrm{Au},i+1}) - (j_{\mathrm{Al},i} - j_{\mathrm{Al},i+1}) x_{\mathrm{Au},i+1}] \\ v_{i+1} &= \frac{\Omega_{i+1}}{x_{\mathrm{Au},i} - x_{\mathrm{Au},i+1}} [(j_{\mathrm{Au},i} - j_{\mathrm{Au},i+1})(1 - x_{\mathrm{Au},i}) - (j_{\mathrm{Al},i} - j_{\mathrm{Al},i+1}) x_{\mathrm{Au},i}] \end{aligned} \tag{11}$$

in a reference frame where the local lattice is at rest (cf. Ref. [23]). The thickening rates of each phase can be inferred from Eq. (11) using:

$$\dot{d}_i = u_i - v_i \tag{12}$$

Now Eq. (10), with Eqs. (8), (9) and (12) inserted, represents a system of linear equations for the fluxes with the boundary conditions that no reaction takes place at the leftmost and rightmost boundaries, $v_1 = u_n = 0$, and the fluxes in the terminal phases are zero:

$$j_{Al,0} = j_{Al,n} = j_{Au,1} = j_{Au,n} = 0 \quad (13)$$

It remains to integrate the evolution equations for the displacement rates over the time, which is done numerically.

3. Results

Crystallographic information on all treated stoichiometric phases in the Al–Au-system was taken from the ICSD database [54], as shown in Table 1. All atomic positions were allowed to relax until the maximum force on any atom was below 0.001 Rydberg/bohr, i.e. less that 0.03 eV/Å. In the case of vacancy calculations in the compound Al_2Au, we additionally optimized the lattice constants, but this had negligible effect on the calculated formation energies. For the reference systems of pure fcc bulk Al and Au, the calculated lattice constants are 3.97 Å for aluminium and 4.07 Å for gold, which are in good agreement with other calculations using LDA (3.99 Å[55] and 4.06 Å[56] for Al and Au, respectively). Experimental values are 4.04 Å for aluminium [57] and 4.07 Å for gold [58].

3.1. Formation enthalpies of low-temperature Al–Au intermetallics

The calculation of formation enthalpies from first principles provides information about the thermodynamic behaviour of the intermetallics at equilibrium and phase stability. To check convergence, two different sets of calculations were done, with two cut-off energies of $E_{cut} = 218$ and 300 eV. Note that in the calculations we have ignored any contributions from temperature and pressure.[1] Results for ΔH_F according to Eq. (1) are given in Table 2 and compared to experimental data in Fig. 3. As can be seen, a good agreement is obtained. The values of all the calculated formation enthalpies, with the only exception of β-$AlAu_2$, lie on a convex curve (see Fig. 3), and the respective compounds are thus expected to be stable equilibrium phases, in accordance with experiment [59]. Phases with energies above this convex envelope are unstable with respect to decomposition into other phases. Therefore our calculated data give a more consistent representation of observed low-temperature phase stability than the experimental values from either Ref. Ferro et al. [51] or Ref. Predel and Ruge [52], while being more complete than Smithells Metals Reference Book [53]. We note in addition that in the experimental works [51–53] the observed modification of $AlAu_2$ was not further specified as α- or β-$AlAu_2$. Our results indicate that, at a stoichiometric composition of precisely 1:2, α-$AlAu_2$ is the prevailing phase at low T.

[1] Ambient pressure in reality is close enough to zero pressure in theory, hence $\Delta H_F \approx \Delta E_F$ is a good approximation.

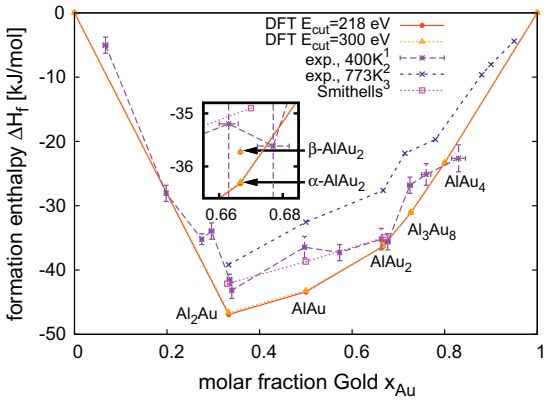

Fig. 3. DFT formation enthalpies of the low-temperature phases in the Al–Au-System at 0 K compared to experimental data: (1) from Ref. [51], (2) from Ref. [52] and (3) from Ref. [53]. For our DFT calculations, the lines form a convex envelope, while the lines between experimental data only serve as a guide.

3.2. Vacancy formation energies

Vacancy formation energies in the compounds Al_2Au, AlAu and $AlAu_4$ were calculated according to Eq. (2), with a plane wave cut-off at 218 eV. Table 3 and Fig. 4 show the results. There is a clear trend that the formation energies for gold vacancies are inversely correlated to the gold content. For gold-rich condition, the formation energy drops from 2.85 eV in the most aluminium-rich compound Al_2Au to only 0.55 eV on a **b** position in the most gold-rich compound $AlAu_4$. For aluminium-rich conditions (Fig. 4b), the E_V change by not more than 0.1 eV in AlAu and $AlAu_4$. In Al_2Au, the vacancy formation energy of gold is 0.34 eV lower and that of aluminium is 0.55 eV higher when compared to gold-rich conditions. In $AlAu_4$, vacancy formation energies for aluminium are significantly higher than those for gold, irrespective of the chosen chemical equilibrium.

In order to explore the effect of the size of the unit cell on the vacancy formation energies, additional calculations were carried out for the cubic compounds Al_2Au and $AlAu_4$ using an fcc supercell with twice as many atoms as in the simple cubic (sc) supercell and correspondingly greater inter-vacancy distance, d_V. As Table 3 shows, the resulting differences of the formation energies are relatively small.

3.3. Nearest neighbour jumps in $AlAu_4$

For each vacancy, a list of possible jumps leading to an exchange between the vacancy and one of its nearest neighbours is required. We first look at the local nearest-neighbour environment of all the prototype atoms in the unrelaxed bulk structure. There are three different prototype atoms in $AlAu_4$: Al and Au on Wyckoff position **a** (4 equivalent atoms each), and Au on Wyckoff position **b** (12 equivalent atoms). There are 10 unique pairings of nearest neighbours in the structure, with bond lengths

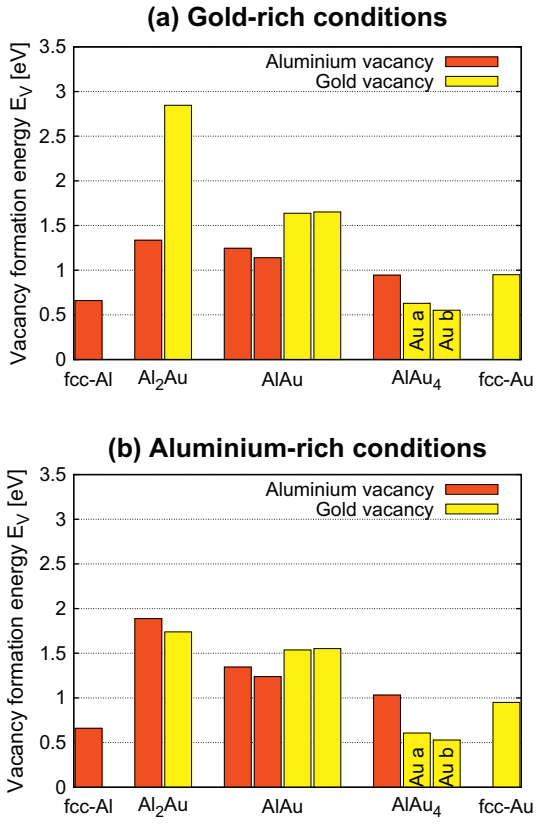

Fig. 4. Comparison of aluminium and gold vacancy formation energies in Al_2Au (fcc supercell with 23 atoms), AlAu and $AlAu_4$ (fcc supercells with 39 atoms each) under (a) gold-rich and (b) aluminium-rich conditions. Multiple bars for one element indicate vacancies at non-equivalent lattice sites.

ranging between 2.59 and 3.02 Å.[2] Four of these pairings involve an aluminium and a gold atom, allowing two different scenarios: aluminium jumping into a gold vacancy or vice versa. Hence, we arrive at 14 different calculations needed to treat all possible nearest neighbour jumps involving a single vacancy. There are no nearest-neighbour jumps of Al atoms into Al vacancies because the sites on the aluminium sublattice are completely screened by gold atoms. The various jumps are summarized in Table 4.

The NEB method is used to calculate the minimum energy trajectories and saddle point energies of each of these elementary diffusion processes. Since a cut-off energy $E_{cut} = 218$ eV has been shown to give good convergence, we use this value and Monkhorst–Pack k-point samplings of $k_{xyz} = 2 \times 2 \times 2$. The results of all calculations are summarized in Fig. 5 and Table 4. The lowest barrier is 0.27 eV, corresponding to an Au **b** atom jumping to the nearest Au vacancy (jump type No. 5 in Table 4), while the largest barrier is 1 eV, corresponding to an Au **b** atom jumping to a nearest Al vacancy site (jump type No. 10).

[2] One pairing, which has a significantly longer distance of 3.57 Åand completes the 14-fold coordination of Au **b**, has not been included in our calculations.

Note that, for all jumps involving an Al atom moving to a nearest Au site, the final energy is much higher, as shown in Fig. 5c, since these jumps create an Al–Au anti-site defect, in addition to an Al vacancy. The results of Fig. 5c also indicate that the Al atom "sees" a much smaller barrier for the jump going backwards than forwards. Hence we already expect Al diffusion to be strongly supressed relative to Au diffusion in $AlAu_4$.

3.4. Tracer diffusion coefficients

The calculation of tracer diffusion coefficients from vacancy hopping rates in ordered intermetallic compounds is a complicated task, the solution of which generally requires kinetic Monte Carlo or equivalent simulation methods [45–48]. Instead of applying numerical methods, we develop an approximate closed-form solution, which illustrates the physics of the diffusion process in $AlAu_4$.

First it is assumed that the high anti-site defect energies prevent atoms from moving to the sublattice of the other species. This means that, within this approximation, Al cannot diffuse in $AlAu_4$ at all, since aluminium atoms are surrounded by gold atoms. Higher-order diffusion mechanisms, e.g. six-jump cycles [47,60], which re-establish the chemical order after a certain number of steps, are not considered. The analysis of a six-jump cycle would require additional DFT calculations for the intermediate steps in which anti-site defects are created and annihilated.

It is reasonable to assume that jumps with high activation barriers do not contribute substantially to diffusive transport and can therefore be ignored. According to Table 4 the most favourable jump types that do not create anti-site defects are type No. 5, with 0.27 eV activation energy, type No. 8, with 0.44 eV, and type No. 12, with 0.48 eV. All of these jumps take place between sites on the Au b sublattice, and none of them alone provides a contiguous path for long-range diffusion. Fig. 6 illustrates the situation. There are triplets of sites that are connected by either type-5, type-8 or type-12 jumps. The triplets are arranged in isolated triangles, which are connected at their corners with the triangles of the two other types. Gold atoms can move easily within the type-5 triangles, but for long-range diffusion they need to jump between these triangles, with significantly higher migration energies of 0.44 or 0.48 eV.

Hence one can consider the centres of gravity of the type-5 triangles as the lattice sites of an elementary diffusion model. These triangular "traps" are coordinated sixfold, with distances of 4.24 Å. Because all the triangles are equivalent (they can be transformed into each other by the symmetry operations of a Wyckoff **a** position), and there are only two jumps to be considered (leading to four jump rates, backward and forward), the calculation of gold diffusion simplifies considerably.

To calculate the (scalar) diffusion coefficient for cubic crystals, we start from the relationship [61]

$$D^* = f\frac{\Gamma\langle r^2\rangle}{6} \tag{14}$$

Table 4
List of jump types, jump distances α, jumping atoms and vacancy types, forward and backward jump energies and attempt frequencies.

Jump type	Jump distance α (Å)	Atom type	Vacancy type	Activation energy		Attempt frequency	
				$E_{\rightarrow}$ (eV)	$E_{\leftarrow}$ (eV)	$\nu_{\rightarrow,0}$ (THz)	$\nu_{\leftarrow,0}$ (THz)
1	2.59	Al	Au **a**	0.43	0.07	2.59	3.68
2	2.59	Au **a**	Al	0.31	0.28	1.19	1.23
3	2.70	Au **b**	Al	0.50	0.35	1.41	1.21
4	2.70	Al	Au **b**	0.72	0.15	3.60	2.18
5a	2.86	Au **b**	Au **b**	0.27	0.27	1.16	0.85
5b	2.86	Au **b**	Au **b**	0.27	0.27	0.85	1.16
6a	2.88	Au **a**	Au **b**	0.64	0.51	1.48	0.84
6b	2.88	Au **b**	Au **a**	0.51	0.64	0.84	1.48
7a	2.90	Au **a**	Au **b**	0.70	0.57	1.41	0.96
7b	2.90	Au **b**	Au **a**	0.57	0.70	0.96	1.41
8a	2.91	Au **b**	Au **b**	0.44	0.44	1.31	0.97
8b	2.91	Au **b**	Au **b**	0.44	0.44	0.97	1.31
9a	2.92	Au **a**	Au **b**	0.79	0.67	1.67	1.15
9b	2.92	Au **b**	Au **a**	0.67	0.79	1.15	1.67
10	2.93	Au **b**	Al	1.00	0.82	1.83	1.72
11	2.93	Al	Au **b**	0.76	0.22	3.84	2.01
12a	2.95	Au **b**	Au **b**	0.48	0.48	1.24	1.06
12b	2.95	Au **b**	Au **b**	0.48	0.48	1.06	1.24
13	3.02	Au **b**	Al	0.94	0.75	1.59	2.07
14	3.02	Al	Au **b**	0.74	0.25	4.48	2.90

with the total jump rate from a given position Γ, the correlation factor f and the mean squared jump displacement $\langle r^2 \rangle$. Γ is the sum of all the individual jump rates Γ'_i to nearest-neighbour positions i,

$$\Gamma = \sum_{i=1}^{n} \Gamma'_i = x_V \sum_{i=1}^{n} \nu_{\rightarrow,i} \exp \frac{-E_{\rightarrow,i}}{kT} \tag{15}$$

with the vacancy fraction on the Au **b** lattice

$$x_V = \exp \frac{-E_V}{kT} \tag{16}$$

the attempt frequency $\nu_{\rightarrow,i}$ and activation barrier $E_{\rightarrow,i}$ as in Table 4. As a triangle is connected to any of its six neighbouring triangles by two jumps, with the two activation energies of 0.44 and 0.48 eV, it follows $n = 12$ and the values for jumps 8a, 8b, 12a and 12b in Table 4 each enter the sum in Eq. (15) three times.

As the distances between triangle centres are all the same, $\langle r^2 \rangle$ takes a value of $(4.24\ \text{Å})^2 = 18.0\ \text{Å}^2$.

The correlation factor f in Eq. (14) describes the deviation of the diffusion behaviour from an ideal random walk, which occurs because successive jumps are not completely independent in real materials. In fact, atoms that have just moved by a vacancy mechanism are more likely to jump back, thus effectively neutralizing a fraction of the jump rate. Therefore f assumes values between 0 and 1. The approximation for the correlation factor that has been used is [62]

$$f = \frac{1 - P_{\text{back}}}{1 + P_{\text{back}}} \tag{17}$$

with P_{back} denoting the probability of a jumped atom to reverse its movement before the vacancy finally diffuses away. P_{back} is given by

$$P_{\text{back}} = \left(\Gamma'_{8a} + \Gamma'_{12b}\right)/\Gamma \tag{18}$$

in 50% of cases and

$$P_{\text{back}} = \left(\Gamma'_{8b} + \Gamma'_{12a}\right)/\Gamma \tag{19}$$

in the remaining 50%. The mean value of the resulting correlation factors f is 0.71 and has only a negligible dependence on temperature. It is practically identical to the correlation factor that one would expect from Eq. (17) in a sixfold coordinated lattice with uniform jump rates and $P_{\text{back}} = 1/6$, $f = 5/7$.

Expression (14) for the gold tracer diffusion coefficient can be evaluated at variable temperature T, and through an Arrhenius-type plot an effective activation energy and pre-exponential factor can be obtained. In spite of the different activation energies entering into the calculation, the curve in Fig. 7 is linear up to 510 °C. At this temperature, the phase $AlAu_4$ becomes unstable and undergoes a peritectoid reaction into the high-temperature β-phase and Al_3Au_8 [12,59]. The temperature dependency can be described as

$$D^*(T) = A \exp \frac{-E_{\text{act}}}{kT} \tag{20}$$

The pre-exponential factor A and activation energy E_{act} are found from a linear fit to be

$$A = 2.62 \times 10^{-7} \frac{\text{m}^2}{\text{s}} \qquad E_{\text{act}} = 1.00\ \text{eV} = 96.5\ \frac{\text{kJ}}{\text{mol}} \tag{21}$$

The activation energy is slightly greater than the sum of the formation energy of an Au **b** vacancy and the migration energy of a type-8 jump.

3.5. Phenomenological simulation of phase kinetics

In the following, we apply the phenomenological model described in Section 2.3 to the case of an Al–Au interface,

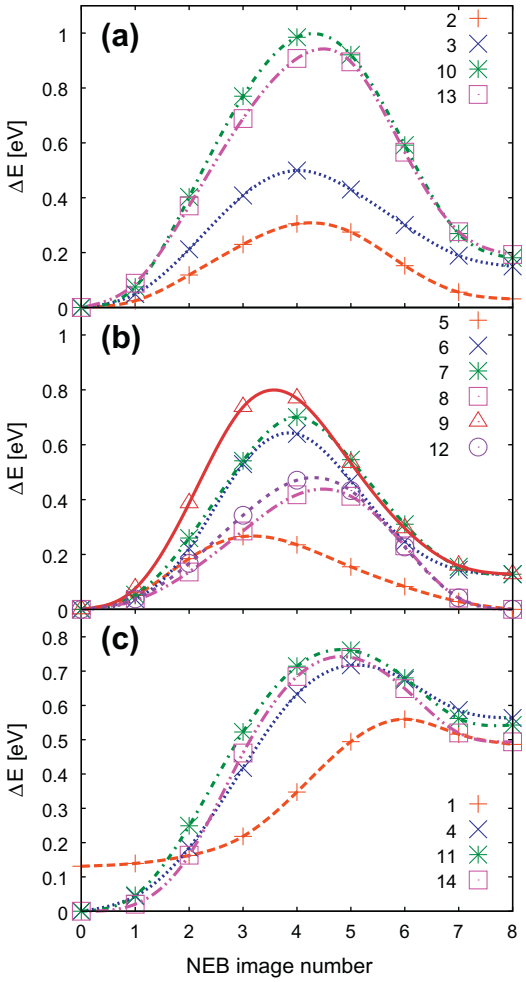

Fig. 5. Energy curves of (a) gold atoms jumping into aluminium vacancies, (b) gold atoms jumping into gold vacancies and (c) aluminium atoms jumping into gold vacancies in $AlAu_4$, as obtained by NEB calculations. In each case, the horizontal axis describes the index of the NEB image. The numbering of the curves is the one used in Table 4 and the lines are spline interpolations. Curve number 1, involving a vacancy on an Au **a**-position, has been offset by 0.13 eV indicating the slightly higher vacancy formation energy of Au **a** compared to Au **b**.

assuming an idealized one-dimensional system of planar phases, as it may be observed in the centre of a thermosonic ball bond contact during ageing. Initially an aluminium layer with 1 μm thickness is covered by a 10 μm thick gold layer. The only compounds allowed to grow at the interface are $AlAu_4$ and Al_3Au_8. This is consistent with observations on modern, miniaturized bond contacts, in which phases like Al_2Au play a minor role as compared to earlier works [4], and occur mostly just in the periphery of the ball bond in the later stages of the reaction.

In the present work, we only calculated the gold diffusion coefficient in the most gold-rich phase $AlAu_4$ atomistically. The aluminium diffusion coefficient, which was not explicitly determined atomistically, is set to a very small value. Further, the diffusion coefficients in Al_3Au_8 are assumed to be the same as in $AlAu_4$, i.e. we use the empirical Cu_3Au rule [63]. As this rule gives a systematic dependence of defect and diffusion properties in binary intermetallics on their composition, it seems reasonable to treat $AlAu_4$ and Al_3Au_8 similarly in this respect, given the small difference in composition and the fact that in both structures there are no Al–Al nearest neighbours.

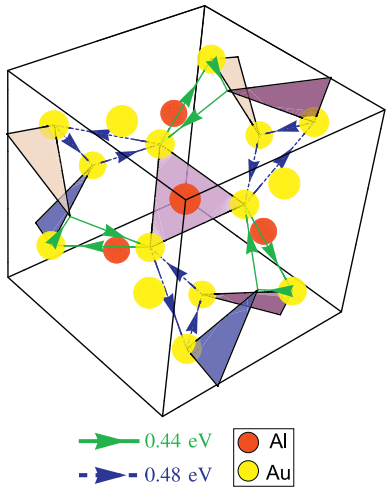

Fig. 6. Local environment of a triangular vacancy trap in $AlAu_4$, as seen along the (1 1 1) direction. Semitransparent triangles are type-5, with low activation energies of $E_{\rightarrow} = 0.27$ eV. Green and blue dotted arrows denote jumps of type-8 and type-12, with 0.44 and 0.48 eV activation energies, respectively. Jumps in the direction of the arrows are of type a (see Table 4). (For interpretation of the references to colour in this figure legend, the reader is referred to the web version of this article.)

The molar Gibbs energies of the involved phases were set to their formation enthalpies. Since in our model there is no diffusion in the terminating phases of the system, no diffusion coefficients in the fcc-Al and fcc-Au phases are needed. The molar volumes for all phases were set to 1.0×10^{-5} m^3 per mol and are not expected to influence the diffusion noticeably, as all stresses from volume changes can relax in the considered planar idealization.

The result of the simulation for a constant temperature of 175 °C is shown in Fig. 8. From the beginning of the

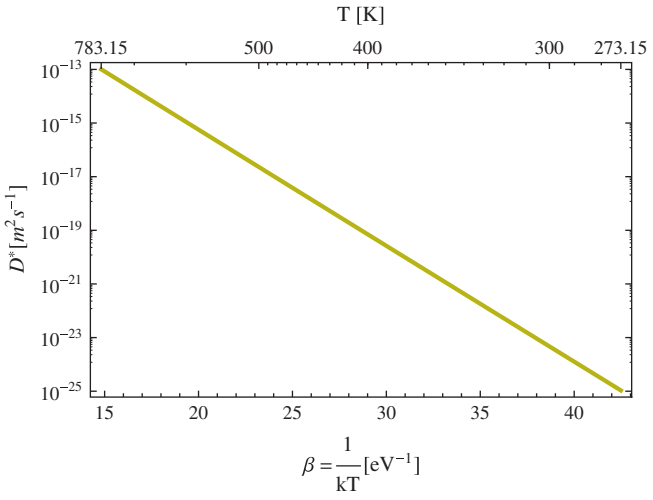

Fig. 7. Arrhenius plot of the gold tracer diffusion coefficient D^* in $AlAu_4$, as calculated from Eq. (14) in the temperature range 0 °C $\leqslant T \leqslant$ 510 °C.

reaction, both allowed intermetallic compounds exhibit a parabolic growth behaviour in time, leading to straight lines in the plot of d vs. $\sqrt{t}$. In this initial stage, the phase Al_3Au_8 grows considerably faster than $AlAu_4$, which can be attributed to its lower formation enthalpy of $-29\ kJ\ mol^{-1}$ compared to $-23\ kJ\ mol^{-1}$ for $AlAu_4$, as the diffusion coefficients were chosen to be the same and the compositions are similar.

4. Discussion

In the presented version of the phenomenological model, all the allowed intermetallic phases whose molar free energies are along the convex envelope of Fig. 3 nucleate at the same time at the very beginning of the simulation and grow concurrently. Due to the assumptions made in the model, which neglects any limitation of the reaction rate at the intermetallic interfaces, this growth behaviour is expected and conforms with well-known results from studies of reactive diffusion in a purely diffusion controlled regime [64,65].

A drastic change in kinetics occurs as soon as the aluminium has been consumed after about 112 h (marked with a black vertical line in Fig. 8). From then on, the growth rate of $AlAu_4$ accelerates at the expense of Al_3Au_8, which now serves as the source of aluminium for the continued evolution of the system. This is in qualitative agreement with experimental results [20,66], where, after the consumption of the aluminium, a thick layer of Al_3Au_8 gets converted to $AlAu_4$. In these experiments, it was found that the $AlAu_4$ grows mainly at its interface with the more Al-rich phase, while voids and interfacial flakes remain embedded close to the interface with the gold wire. If one interprets these features as marker particles to visualize a Kirkendall shift, this is exactly the behaviour expected for compounds where diffusion of gold is the dominant transport mechanism and hardly any aluminium diffuses. Our approximation that the diffusivity of aluminium can be ignored and there is no aluminium in the fcc gold phase clearly reproduces this behaviour with the employed mass balance equations: inserting $j_{Al,i} = 0$ and Eq. (13) into Eq. (11) yields an expression for the growth velocity at the gold-rich end of the $AlAu_4$ phase,

$$u_{n-1} = \frac{\Omega_{n-1}}{x_{Au,n-1} - x_{Au,n}}(1 - x_{Au,n}) j_{Au,n-1} \tag{22}$$

with $n = 4$ before and $n = 3$ after the consumption of the aluminium layer. Since $x_{Au,n} = 1$, this velocity is zero and the $AlAu_4$ phase only grows on the aluminium-rich side, while any markers on the gold-rich side, like oxide flakes or pores, remain at their position close to the Au–$AlAu_4$ interface.

In spite of this qualitative agreement with experimental observations, the timescale of the reactions is not the same. Specifically, our predicted time of complete consumption of the Al layer of $(636)^2 s = 112$ h is about a factor of 10 longer than the reported value of 11 h [20]. The most likely of several possible explanations appears to be that diffusion along grain boundaries or other lattice defects may be substantially faster than in the ideally ordered intermetallic bulk phases, in particular because of the presence of columnar grains in both Al_3Au_8 and $AlAu_4$.

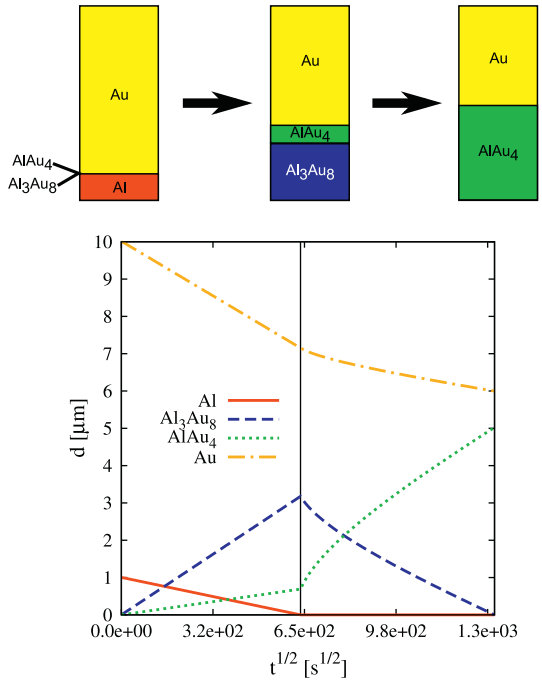

Fig. 8. Time dependence of phase thicknesses of a planar diffusion sample as obtained from the phenomenological model. The initial condition was $d_{Al} = 1\ \mu m$, $d_{Al_3Au_8} = 10$ nm, $d_{AlAu_4} = 10$ nm and $d_{Au} = 10\ \mu m$. The black vertical line indicates the time when the pure aluminium layer is completely consumed and the phase kinetics start deviating from the ideal parabolic behaviour.

5. Summary and conclusions

Our focus in the present work has been the investigation of reactive diffusion in thermosonic contacts of gold wires on aluminium bond pads. We have presented a simple but effective method for modelling phase reaction kinetics which couples atomistic calculations, based on DFT, to large-scale phenomenological continuum models, based on Onsager's extremal principle. DFT calculations were used to investigate the thermodynamic stabilities of various Al_xAu_y intermetallic phases via the calculation of the formation enthalpies. Our results show that Al_2Au is the most stable, and has the lowest formation enthalpy, in agreement with experimental caloric measurements, and that the α-$AlAu_2$ phase is more stable than β-$AlAu_2$. Altogether, our calculated formation enthalpies give a more consistent representation of experimental results, demonstrating the power of DFT calculations in augmenting experimental data, e.g. as input to CALPHAD databases. The DFT method was also used to study vacancy-mediated diffusion mechanisms on the atomic scale. Atomic migration paths and barriers were investigated using the NEB

method. Our results indicate that the empirical Cu_3Au rule, which predicts the more abundant species in intermetallic compounds to be the more mobile one, is clearly justified for aluminium–gold compounds. An approximate model for the calculation of tracer diffusion coefficients from the vacancy jump rates in $AlAu_4$ is developed. The essence of the model is that the vacancy jumps with the smallest activation energy occur in closed triangles and therefore do not support long-range diffusion. Rather, long-range diffusion is controlled by jumps between these triangles. The atomistically calculated diffusion coefficient and formation enthalpies are then used as input data for a phenomenological simulation of the growth behaviour of $AlAu_4$ and Al_3Au_8 at the aluminium–gold interface in a multilayer model for the system bond pad–wire–ball at 175 °C. In agreement with results from experiments [20] for alloy systems, we obtained a rapid growth of the Al_3Au_8 phase in the initial stage of ageing. Upon complete consumption of the aluminium film, the Al_3Au_8 phase transforms into the $AlAu_4$ phase. In this final stage, the main reaction is that of Al_3Au_8 with gold that diffuses through the $AlAu_4$ phase, while the contribution of aluminium diffusing to the Au–$AlAu_4$ interface to $AlAu_4$ phase growth is negligible. This unbalanced diffusion is expected to cause further phenomena related to the Kirkendall effect, like pore growth on the Au–$AlAu_4$ interface weakening the bond contact. Further work on the determination of kinetic data of further Al–Au phases in addition to $AlAu_4$ is in progress.

Acknowledgements

J.S. gratefully acknowledges the financial support by the Czech Science Foundation in the frame of project P204/10/1784. The authors thank Prof. Matthias Petzold for helpful discussions.

References

[1] Adam J, et al. International technology roadmap for semiconductors – assembly and packaging; 2009. <http://www.itrs.net/Links/2009ITRS/2009Chapters_2009Tables/2009_Assembly.pdf>.
[2] Karpel A, Gur G, Atzmon Z, Kaplan WD. J Mater Sci 2007;42:2334–46.
[3] Philofsky E. Reliab Phys Symp 1971;120–8 [9th Annual].
[4] Philofsky E. Solid-State Electron 1970;13:1391–9.
[5] Breach CD, Wulff FW. Microelectron Reliab 2010;50:1–20.
[6] Karpel A, Gur G, Atzmon Z, Kaplan WD. J Mater Sci 2007;42:2347–57.
[7] Malone DW, Hummel RE. Crit Rev Solid State Mater Sci 1997;22(3):199–238.
[8] Mishin Y, Herzig C. Mater Sci Eng A 1999;260:55–71.
[9] Smigelskas AD, Kirkendall EO. Trans AIME 1947;171:130–42.
[10] Klengel R, Knoll H, Petzold M, Wohnig M, Schräpler L. In: Electronics Systemintegration Technology Conference, 2006. 1st. IEEE; 2006. p. 370–5.
[11] Müller T, Schräpler L, Altmann F, Knoll H, Petzold M. Electronics Systemintegration Technology Conference, 2006. 1st, Vol. 2. IEEE; 2006. p. 1266–73.
[12] Murray JL, Okamoto H, Massalski TB. Bull Alloy Phase Diagr 1987;8(1):20.
[13] Blech IA, Sello H. J Electrochem Soc 1966;113(10):1052–4.
[14] Hanai M, Houkyou M, Utiyama N, Fuwa A. J Jpn Inst Met 1996;60(1):37.
[15] Majni G, Ottaviani G, Galli E. J Cryst Growth 1979;47:583–8.
[16] Majni G, Nobili C, Ottaviani G, Costato M, Galli E. J Appl Phys 1981;52(6):4047.
[17] Weaver C, Brown LC. Philos Mag 1962;7:1–16.
[18] Weaver C, Parkinson DT. Philos Mag 1970;22(2):377.
[19] Breach CD, Tok CW, Wulff F, Calpito D. J Mater Sci 2004;39:6125–8.
[20] Breach CD, Wulff FW. Gold Bull 2009;42:92.
[21] Zhang L, Du Y, Ouyang Y, Xu H, Lu XG, Liu Y, et al. Acta Mater 2008;56:3940–50.
[22] Svoboda J, Turek I, Fischer FD. Philos Mag 2005;85(31):3699–707.
[23] Svoboda J, Gamsjäger E, Fischer FD, Kozeschnik E. J Phase Equilib Diffus 2006;27(6):622.
[24] Straumanis ME, Chopra KS. Z Phys Chem 1964;42:344–50.
[25] Frank K, Schubert K. J Less–Common Met 1970;22:349.
[26] Pušelj M, Schubert K. J Less–Common Met 1974;35:259–66.
[27] Range KJ, Büchler H. J Less–Common Met 1989;154(2):251–60.
[28] Büchler H, Range KJ. J Less–Common Met 1990;161:347–54.
[29] Iijima Y, Nakajima K, Hirano K. Mater Trans JIM 1989;30(7):480–6.
[30] Onsager L. Ann NY Acad Sci 1945;46:241.
[31] Svoboda J, Fischer FD, Abart R. Acta Mater 2010;58:2905–11.
[32] Palade P, Wagner FE, Jianu AD, Filoti G. J Alloy Compd 2003;353(1–2):23–32.
[33] Hohenberg P, Kohn W. Phys Rev 1964;136:B864.
[34] Kohn W, Sham LJ. Phys Rev 1965;140:A1133.
[35] Perdew JP, Zunger A. Phys Rev B 1981;23:5048.
[36] Vanderbilt D. Phys Rev B 1985;32:8412.
[37] Elsässer C, Takeuchi N, Ho KM, Chan CT, Braun P, Fähnle M. J Phys: Cond Matter 1990;2:4371–94.
[38] Lechermann F, Welsch F, Elsässer C, Ederer C, Fähnle M, Sanchez JM, et al. Phys Rev B 2002;65:132104.
[39] Lechermann F, Fähnle M, Meyer B, Elsässer C. Phys Rev B 2004;69:165116.
[40] Monkhorst HJ, Pack JD. Phys Rev B 1976;13:5188.
[41] Fu CL, Ho KM. Phys Rev B 1983;28:5480.
[42] Jónsson H, Mills G, Jacobsen KW. In: Berne BJ, Ciccotti G, Coker DF, editors. Classical and quantum dynamics in condensed phase simulations. World Scientific; 1998. p. 385–404.
[43] Zhang SB, Northrup JE. Phys Rev Lett 1991;67(17):2339–42.
[44] Hine NDM, Frensch K, Foulkes WMC, Finnis MW. Phys Rev B 2009;79:024112.
[45] Bakker H, Westerveld JPA. Phys Status Solidi (b) 1988;145:409–17.
[46] Belova IV, Murch GE. J Phys Chem Solids 1999;60:2023–9.
[47] Belova IV, Murch GE. Defect Diffus Forum 2004;224–225:45–52.
[48] Van der Ven A, Ceder G, Asta M, Tepesch PD. Phys Rev B 2001;64:184307.
[49] Xu Q, Van der Ven A. Acta Mater 2011;59:1095–104.
[50] Svoboda J, Turek I. Philos Mag B 1991;64(6):749–59.
[51] Ferro R, Capelli R, Marazza R. Atti Accad Naz Lincei, Ser VIII, Rend, Cl Sci Fis Mat Nat 1966;41(1–2):85–9.
[52] Predel B, Ruge H. Z Metallk 1972;63(2):59–63.
[53] Brandes EA, Brook GB, editors. Smithells Metals Reference Book. Elsevier; 1998.
[54] Belsky A, Hellenbrandt M, Karen VL, Luksch P. Acta Crystallogr B 2002;58:364–9.
[55] Bross H. Eur Phys J B 2004;37:405–11.
[56] Mehl MJ, Papaconstantopoulos DA. Phys Rev B 1996;54:4519.
[57] Cooper AS. Acta Crystallogr 1962;15:578.
[58] Kittel C. Introduction to solid state physics. John Wiley & Sons; 1953.
[59] Okamoto H. J Phase Equilib 1991;12:114.
[60] Elcock EW, McCombie CW. Phys Rev 1958;109:605.
[61] Balluffi RW, Allen SM, Carter WC. Kinetics of materials. Wiley; 2005.
[62] Mehrer H. Diffusion in Solids. Springer; 2007.

[63] d'Heurle FM, Gas P, Lavoie C, Philibert J. Z Metallk 2004;95(10):852–9.
[64] van Loo FJJ, Rijnders MR, Rönkä KJ, Gülpen JH, Kodentsov AA. Solid State Ion 1997;95:95–106.
[65] Philibert J. Appl Surf Sci 1991;53:74–81.
[66] Breach CD, Wulff F. Microelectron Reliab 2004;44:973–81.